Soft Matter

Stimuli-responsive gel impregnated surface with switchable lipophilic/oleophobic properties

Journal:	*Soft Matter*
Manuscript ID	SM-ART-10-2019-002016.R1
Article Type:	Paper
Date Submitted by the Author:	26-Dec-2019
Complete List of Authors:	Li, Zhenghong; Harbin Institute of Technology Liu, Yingzhi; Harbin Institute of Technology Lei, Ming; Harbin Institute of Technology Su, Ansu; Northumbria University, Faculty of Engineering and Environment Sridhar, Sreepathy; Northumbria University, Faculty of Engineering and Environment Li, Yifan; Northumbria University, Faculty of Engineering and Environment Liu, Xuqing; University of Manchester, School of Materials Lu, Haibao; Harbin Institute of Technology Fu, Yong Qing; Faculty of Engineering and Environment, Maths, Physics and Electrical Engineering Xu, Ben; Northumbria University, Mechanical and Construction Engineering

ARTICLE

Stimuli-responsive gel impregnated surface with switchable lipophilic/oleophobic properties

Received 00th January 20xx,
Accepted 00th January 20xx

DOI: 10.1039/x0xx00000x

Zhenghong Li [a], Yingzhi Liu [a], Ming Lei [a], Ansu Sun [b], Sreepathy Sridhar [b], Yifan Li [b], Xuqing Liu [c], Haibao Lu *[a], Yong Qing Fu [b] and Ben Bin Xu *[b]

In this paper, we developed a novel morphing surface technique consisting of 3D printed miniature groove structure and injected stimuli-responsive hydrogel pattern, which is capable of switching between lipophilicity and oleophobicity under certain stimuli. Under swelling, the geometrical change of hydrogel will buckle the surface due to the structural confinement and create a continuous transition of surface topology. Thus, it will yield a change on surface wetting property from oleophilic to super-oleophobic with a contact angle of oil of 85° to 165°. We quantitatively investigate this structure-property relationship using finite element analysis and analytical modeling, and the simulation results and the modeling are in good agreement with the experimental ones. This morphing surface also holds its potentials to be developed into autonomous system for future sub-sea/off-shore engineering applications to separate oil and water.

1 Introduction

Developing novel and controllable wettability approaches using functional surfaces has attracted significant research interests, with underwater super-oleophobic surfaces being one of the hottest areas with promising applications in micro-fluidics, oil/water separation, marine antifouling coating, and self-cleaning technology.[1-7] For example, Jiang's group previously found an interesting phenomenon from fish, where its self-cleaning skin has a multi-length-scale hierarchical structure to enable an outstanding under water oleophobic property and on-demand surface wettability control, thus allowing fish to move freely in the oil-contaminated water.[8]

Aizenberg et.al developed a rough structure to lock the liquid to prepare a smooth liquid-infused porous surface (SLIPS), inspired by the structure of the pitcher plant.[9] This surface is good at reducing the viscous force of the liquid on the surface and can repel all liquids. Lu et al. prepared TiO_2 particles of two different sizes and ethanolic suspension with a certain proportion of fluorosilicone, using spray or dip coating methods to adhere them to the surface with double-sided tape. The surface was then immersed in hexadecane to obtain a tough, ultra-smooth and superhydrophobic material.[10] Rykaczewski et al. made micro-pattern arrays on silicon using the photolithography method, then the arrays were post-processed with octadecyltrichlorosilane hydrophobic layer, before infused the surface with ultra-light lubricating oil after adding perfluoro oil. This effectively prompts the droplet condensation of liquid with low surface tension.[11]

Bio-compatible and stimuli-responsive hydrogel materials can sense the environmental changes with adjustable responses controlled by their compositions and physical properties. Suo et al. demonstrated a hydrogel interferometer with adaptive colouration, providing a facilely tuneable way for broader functionalities.[12] Moreover, hydrogels are consisted of unique hydrophilic groups, whose internal three-dimensional (3D) crosslinked polymer network can absorb and retain large amounts of water molecules, which opens up opportunities for interface/surface structure designs to be applied in aqueous environment. For example, Liu's group used hydrogels to simulate fish scales' surfaces, which can be used in underwater super-oleophobic surface.[13,14] The conventional approach for oil/water separation is heavily relied on the hydrophilic nature of materials, *e.g.* using the hydrogel structures for oil/water separation.[15-17] However, the surfaces of such structures can be easily contaminated by oil residues, while the fabrication cost is normally high.

Recently, additive manufacturing, *e.g.* 3D printing, have re-invented the rapid prototyping technologies with a great efficiency.[18] Whilst there are great application potentials, some technical challenges remain, such as facilitation of complicated geometries and printing precisions. Currently, researchers have applied soft functional materials together with structural designs for enhanced actuating/sensing.[19,20] For example, Lewis et al fabricated strain sensors within highly conformal and extensible elastomeric matrices.[21] Kang et al printed integrated structures of a hydrogel and an elastomer in an arbitrary sequence, which enables new soft robotics concepts for medicine engineering.[22] Lei et al used 3D printing to achieve an auxetic metamaterial, which can continuously

[a] State Key Laboratory of Science and Technology on Advanced Composites in Special Environments, Harbin Institute of Technology, Harbin 150080, P.R. China.
[b] Smart Materials and Surfaces Laboratory, Faculty of Engineering and Environment, Northumbria University, Newcastle upon Tyne NE1 8ST, UK.
[c] School of Materials, University of Manchester, Oxford Road, Manchester, United Kingdom, M13 9PL.
† E-mail: luhb@hit.edu.cn and ben.xu@northumbria.ac.uk

tailor its in-plane moduli and Poisson's ratios by utilizing the shape memory effect of hydrogels.[23]

There have been a number of studies to achieve hydrophilic-hydrophobic control and transition on surface by combining material properties and surface topography.[24-26] For example, Yuan et al. prepared flexible structures by coating leaf-shaped zeolitic imidazolate framework (ZIF-L) materials on a 3D printed surface to achieve a super hydrophobicity in air and super-lipophilicity in water.[27] However, the concept of using geometrical changes from responsive material to enable a controllable lipophilic/oleophobic transition on surface has yet been reported.[28-30]

In this work, we demonstrate a strategy to achieve a smart hybrid surface by combining 3D printed acrylate-based photopolymer and injected hydrogel embedded micro-structures. The surface wetting behaviour is therefore designable and controllable by the synergistic effect of surface groove geometries and the embedded hydrogel patterns. Owing to the reversible swelling of hydrogel, this hybrid surface can be switched between the oleophilic state and the oleophobic state. Finite element analysis and analytical modelling were also carried out to investigate the swelling behaviours of hydrogel and the dynamic evolution of surface morphology, with a good agreement between experimental, simulation and theoretical results. Successful reversible lipophilic/oleophobic property changes have been demonstrated by controlling the swelling ratios of hydrogel.

2 Design and Material Preparation

The substrate is an acrylate-based photopolymer, VerowhitePlus (VW) from Stratasys Inc. (Edina, MN, USA) fabricated using a multi-material 3D printer (Strasys® Objet 24) from CAD designs created using SolidWorks® (Dassault Systems). The printed parts were then washed by acetone and isopropyl alcohol (IPA), then rinsed in de-ionized (DI) water, before dried using nitrogen gas.

Poly (acrylamide-co-sodium acrylate) hydrogel was synthesized by mixing the acrylamide, sodium acrylate, N, N'-methylenebis(acrylamide) and DI water. The mixture was then agitated and degassed for 10 mins, followed by adding 0.3 µL of N, N, N', N'-tetramethylethylenediamine and 1.0µL of aqueous ammonium persulfate solution to synthesis the gel. Red dye was added into the solution to enhance the visualization.

Table 1. 3D model dimensions and contact angles

W_{gel}(mm)	W_d(mm)	h(mm)	Contact Angle(°)
0.5	0.5	0.5	110.99
0.8	0.5	0.5	107.88
1.0	0.5	0.5	110.55
1.0	1.5	0.8	96.7
1.0	2.0	0.8	95.2
1.0	2.5	0.8	83.32

For comparative studies, plain and smooth hydrogel films were also created, the gel solution was poured into a reaction cell composed of two parallel-separated glass slides with a 300-µm-thick Kapton film spacer to create the gap in-between. The gelatinization of gel solution was kept in the air for 30 mins.

To create hybrid groove-hydrogel surface structures, the designed groove structures were firstly generated on 3D printed substrates (30 mm x 10 mm in size) (Fig. 1). The groove widths range from W_{gel} =0.5-1.0 mm, with a depth of h=0.5-0.8 mm, and distance/pitch between each groove is W_d=0.5-2.5 mm. All the parameters are listed in Table 1. The hydrogel solution was injected into the grooves via precisely positioned syringes aided by Finnpipette F1, and the mould was then placed into the tube. The water was added from the edge, and the device was kept horizontally for 6 hours. Oxygen plasma treatment[31] was then used to enhance the adhesion between hydrogel and substrate (Fig. 1G).

3 Experiments and Results

Surface morphology of the hybrid groove-hydrogel structures can be significantly changed responding to stimuli-responsive gel swelling, which creates an intelligent surface potentially used for oil-water separation. The contact angles of oil droplet are changed by this swelling effect and the separation of oil and water can be expected (Fig. 1).

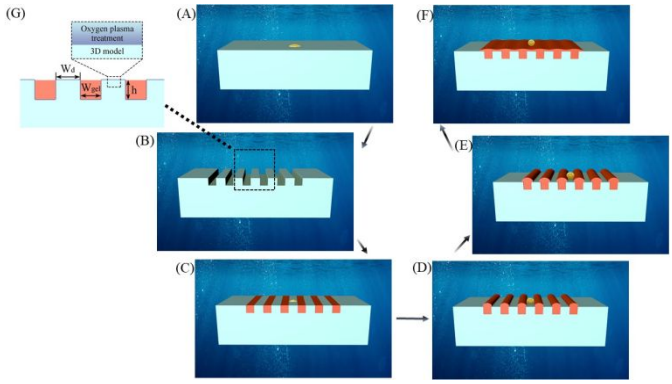

Fig. 1 A) Oil droplet on a smooth 3D surface, B) 3D printing structure, C-F) Demonstrate the process of transforming a smart surface from oleophilic to super oleophobic, G) Oxygen plasma treatment and 3D model scale identification.

A KRUSS® DSA 30S Drop Shape Analyser was used to measure the surface contact angles of oil droplets on plain substrate, hybrid groove-hydrogel surfaces, and plain hydrogel film, in both air and underwater. The organic solvent of 1,2 dichloroethane (wt% = 1.26g/cm^3) was used to prove smart surfaces changing from lipophilic to oleophobic.

We firstly characterized the wetting behaviour on plain and smooth surfaces. In open air, the measured contact angles of oil droplets on the 3D printed smooth plain substrate and wet plain hydrogel film were 53° and 21.1°, respectively. Under water, the contact angle of oil droplet on the 3D printed smooth substrate surfaces was 48.9°, whereas on the fully wetted hydrogel film, the contact angle was close to 165° (Fig. 2A). Therefore, the smooth substrate surface presents a hydrophilic/oleophilic property in the air and under the water, respectively. The contact angles were decreased with the increase of solid surface fraction (Fig. 2B).

On the hybrid surfaces, the surface wetting can be designed by using the changes of surface structures. The fraction of the solid surface area can be calculated by equation (1):

$$f = \frac{W_d}{W_d + W_{gel}} \quad (1)$$

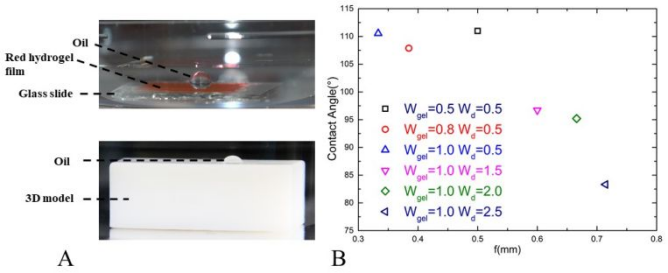

Fig. 2 A) An oil droplet sits on the hybrid surface. B) The contact angle summary of oil/hybrid surface with varied in-plane surface design.

We then characterized the wetting behaviour of the hybrid surface, at its original "smooth" state without any morphology change. After the hybrid surface being treated with (octadecyl) trimethoxy silane (OTMS), the contact angles of water droplets and oil droplets in the air were found to be larger than 90°, revealing the formation of hydrophobic and oleophobic surfaces. The contact angles of oil droplet and water droplet were gradually decreased over time. After 4 hours, the contact angles were changed from the initial value of 102.6° to 83.4° (Fig. 3A and B). The experimental results reveal that the hybrid surface is determined by the hydrophobic and oleophobic properties of the surface treatment. In addition to the chemical treatment, we also introduced geometric designs in order to generate the functions of changes of surface morphology.

Next, the smart surfaces were actuated by immersing the hybrid groove-hydrogel structure in water without other treatment where the swelling hydrogel showed significant changes in the surface morphology (Fig. 3C). The smart surfaces underwent a dynamic swelling change, while the gel swelling ratio became stabilized around its maximum value after 120 mins. Experimental results indicate that the hydrogel experienced a two-stage swelling process. In stage-1, the hydrogel was swelled mainly upwards and behaved like a one-dimensional swelling. In stage-2, the hydrogel followed a two-dimensional swelling until the adjacent gels were contacted and merged with each other, forming a periodic buckling morphology (Fig. 3D).

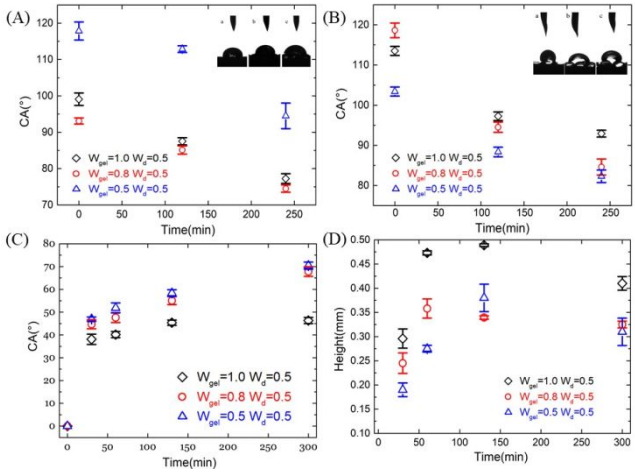

Fig. 3 A) Oleophobic contact angle after surface treatment. B) Hydrophobic contact angle after surface treatment. C) The hydrogel without any treatment swelling morphology. D) The hydrogel swelling height.

We then put 50 μL oil droplet onto the surface. Fig. 4A shows that as the W_d increases, the contact angle decreases. When the W_d value was 2.5mm, the contact angle between substrate and oil droplet was 83.2°, which is oleophilic. For the same groove structure, when the hydrogel became swelling, the contact angles between hydrogel and substrate started decreasing until the oil droplet was separated from the 3D substrate as shown in Figs. 4 A_1 to 4A_4. Meanwhile, the contact angle between hydrogel and the oil substrate were gradually increased when the hydrogel regained its original shape as shown in Figs. 4A_4 to 4A_6.

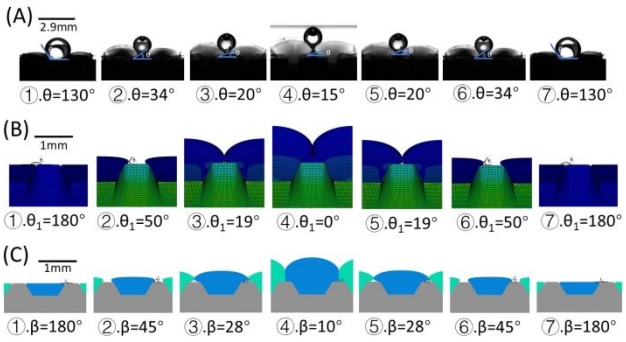

Fig. 4 A) The experimental observation of reversible morphological change during hydrogel swelling/deswelling, θ is three phase contact angle (3D model, hydrogel and water), scale bar is 2.9mm. B) The simulation of the morphology change in hydrogel swelling, θ_1 is three phase contact angle(3Dmodel, hydrogel and water), scale bar is 1mm. c) The simulation of the morphology change in individual hydrogel swelling, β is three phase contact angle (3D model, hydrogel and water), scale bar is 1mm.

4 Theoretical Analysis and Numerical Simulation of Hydrogel Swelling

To further understand the morphology switching, we use finite element method to simulate the process of hydrogel swelling under the confinement from micro-engineered groove. A constitutive model of a neo-Hookean material was used for the hydrogel material. Since the geometric dimension of model was not apparently change along the thickness direction, we used a 2-D plane strain case to reduce the computation time. At a room temperature of 22°C, the 3D printed material is in a glassy state, in which no obvious swelling happens. Considering the smart surface has a periodic structure, we used a half unit and applied a periodic condition. The hydrogel swelling was modelled through monitoring thermal expansion, which was monitored at different normalized times from t=0 (starting point) to t=1 (final stage). The steady analysis only considers the steady water content, and neglects the water gradient. By using this normalized time, the water content is uniformly increased. At the intermediate time t, the water content is 1.5t. That is to say, the gels were not swollen at initial stage of t=0. The gels were fully swollen with a swelling ratio of 1.5 at the final stage where the analysis step was defined as t=1. The structural parameters were set to be W_d = 0.5mm, W_{gel} =1.0mm, h=0.5mm. We used the thermal expansion to mimic the swelling of hydrogel (Figs. $4B_1$~$4B_4$). The initial points before swelling were marked as references and their positions would be continuously changed with the development of swelling, where (X_{gel}, Y_{gel}) was defined as the hydrogel central point and (X_{sub}, Y_{sub}) was defined as the W_d surface middle point. When these two points' distance was reduced, the hydrogel was undergoing its initial swelling period. The changes of this distance vs. time shows the swelling process. Results showed that this distance started to decrease and reached the lowest value at t=0.4401. The distance value was then increased and returned to near the initial value at t=0.8068. From t=0.8068 to t=1 (final stage), the distance was continually increased, eventually the hydrogels on both sides were merged when they were fully contacted with each other.

At the beginning of the swelling of hydrogel, its height remained stable. After t=0.7335, as hydrogel swells and is contacted with each other on both sides, the obtained swelling rates of hydrogel are in accordance with the experimental results (Fig. 5A). In addition, the X, Y coordinates can also be used to calculate the distance between adjacent middle points using equation (2), which helps to understand the 2-stage swelling behaviour observed during the experiments.

$$Z(t)=\sqrt{(X_{gel}(t)-X_{sub}(t))^2+(Y_{gel}(t)-Y_{sub}(t))^2} \quad (2)$$

The two-stage swelling behaviour is originated from changes of morphology from one-dimensional to two-dimensional swelling behaviors have been presented in Figs. 5B~5D. In stage-1 (Fig. 5B and 5C), one-dimensional swelling behaviour occurs because the gel swells upward at the initial stage. The volume deformation of the gel is proportional to the increase of its height, *e.g.*, $dV \propto dh$, where dV is the volume increment per step, and dh is the height increment. L is the hydrogel width. Therefore, the increase of hydrogel's height is a linear function of the time t. During stage-2 of the gel swelling (2D swelling), the upper half of the hydrogel started to form a semicircle (Fig. 5D).

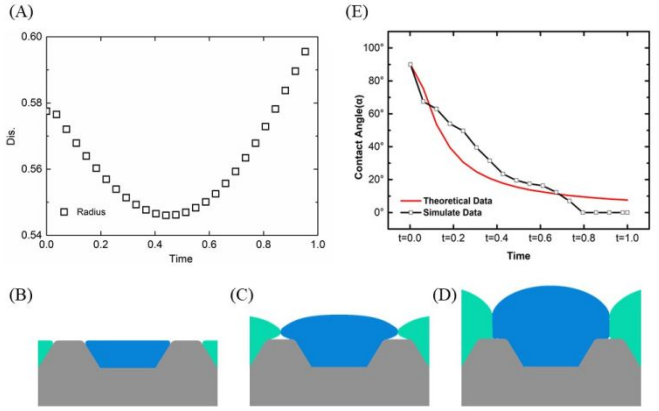

Fig. 5 A) The Z(t) between the center point of the hydrogel and the center point of the W_d surface. B-D) Hydrogel swelling from one-dimensional to two-dimensional. E) theoretical data and simulate data trend.

Therefore, the volume deformation is proportional to the radius increment as shown in equation (3), where R is the radius of the hydrogel, and dR is the radius increment. Therefore, in addition to time, the radius increment is decreased with the increase of R i.e. $\propto 1/R$:

$$dV=\frac{\pi(R+dR)^2-\pi R^2}{2}=\pi\cdot R\cdot dR \quad (3)$$

Figure 6 shows the detailed evolution of surface profiles during the simulated changes of surface morphology induced by the hydrogel swelling process. Before t=0.5428 (plot labelled No. 3), the hydrogel swelled independently. After t=0.5428, hydrogel started to merge with each other to form the adjacent grooves. As hydrogel continued to swell, the gel-gel contact areas were increased gradually. The interaction mode between the contacting hydrogels was set as frictional contact, with a friction coefficient of 0.45 during this simulation.

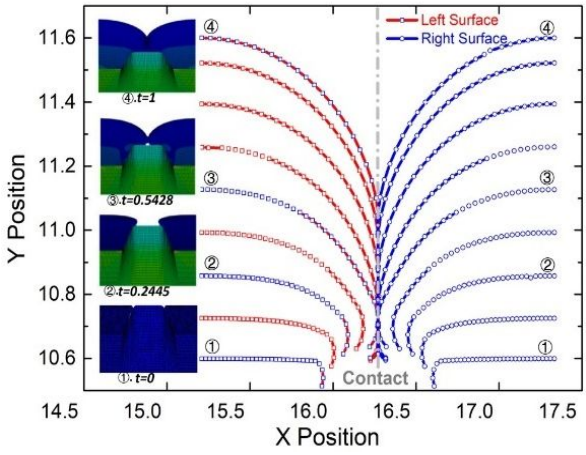

Fig. 6 Hydrogel swelling scale coordinates. Blue squares correspond to the illustration on the left side.

Theoretical analysis of plain hydrogel film swelling without groove structures were also conducted using Equation (4). For this model, *C* is the specific heat capacity, *m* is the quality of the hydrogel, and *T* is the temperature. Assuming no energy loss, the thermal energy will be fully converted into gravitational potential energy and strain energy of the hydrogel. Considering *E* is the elastic modulus, μ is the Poisson's ratio, *S* is the cross-sectional area of the hydrogel, ε is the strain in the direction, γ is the Shear strain, the energy equation (4) can be written as:

$$cmT = mgy + \frac{E}{2(1+\mu)}\left[\frac{\mu}{1-2\mu}(\varepsilon_x+\varepsilon_y)^2 + (\varepsilon_x^2+\varepsilon_y^2)+\frac{1}{2}\gamma XY^2\right]S \quad (4)$$

ϕ is stress function, according to the compatibility equation:

$$\nabla^4\phi = 0 \quad (5)$$

$$u = u(X,Y) = Ax^2 + Bx + Cy^2 + Dy + E \quad (6.1)$$

$$v = v(X,Y) = A_1x^2 + B_1x + C_1y^2 + D_1y + E_1 \quad (6.2)$$

v is an even function about x, $B_1 = 0$, $v = A_1x^2 + C_1y^2 + D_1y + E$;

u is an odd function about x, $A = 0$, $C = 0$, $E = 0$, $u = B_1x$, $v = D_1y$.

When $y = 0$, $v = A_1x^2 + C_1y^2 + D_1Y + E_1$, $v = C_1y^2 + D_1y$:

$$\frac{\partial^2 u}{\partial x^2} + \frac{\partial^2 v}{\partial y^2} = 0 \Rightarrow C_1 = 0 \quad (7)$$

$$\mu = -\frac{\varepsilon_x}{\varepsilon_y} \quad (8)$$

According to Hooke's law:

$$\sigma_x = E\varepsilon_x; \sigma_y = E\varepsilon_y \quad (9)$$

$$\rho ct = \rho gy + \frac{c\rho t}{(1+\mu)(\mu^2+1)}\left[\frac{\mu}{1-2\mu}(-\mu+1)^2 + (-\mu^2+1)\right] \quad (10.1)$$

$$y = \frac{ct - \frac{cT}{(1+\mu)(\mu^2+1)}\left[\frac{\mu}{1-2\mu}(-\mu^2+1)^2 + (-\mu^2+1)\right]}{g} \quad (10.2)$$

$$\alpha = \arctan\frac{d}{y} \quad (10.3)$$

where *d* is the half-length of W_d. α is the angle between substrate and swelling hydrogel. The obtained theoretical results are shown in Fig. 5E, which have similar trends with those from experiments.

5 Conclusions

This paper reports a new design methodology for smart surfaces with hybrid groove-hydrogel structures fabricated by 3D printing and gel injection process. Due to the swelling and expansion of the hydrogel network, the surface morphology of the smart surface can be changed in a controllable manner. Through designed experiments and simulations, we have studied and evaluated the feasibility of oil-water separation mechanisms from this smart surface. During the swelling and merging of hydrogels from the adjacent grooves, the surface was transformed from oleophilic to super-oleophobic. The hydrogel swelling behaviour was carefully evaluated by employing finite element simulations, which shows the switching of swelling mode from one dimensional to two dimensional ones. By using the reversible swelling to achieve the switch between oleophilic and super-oleophobic, we have successfully provided a new method to separate oil and water efficiently.

Conflicts of interest

There are no conflicts to declare.

Acknowledgements

This work is supported by National Natural Science Foundation of China (NSFC) under Grant No. 11672342 and 11725208, the Engineering and Physical Sciences Research Council (EPSRC) grant-EP/N007921/1, and the Newton Mobility Grant (IE161019) through the UK Royal Society and NFSC. Data associated with this paper is available via Northumbria Research Data Management scheme.

References

1 Y. J. Chuang, T. H. Liao, P. R. Chen and K. Y. Hung, *J. Micromech. Microeng.*, 2010, **20**, 085020.
2 S. L. Gras, T. Mahmud, G. Rosengarten and A. Mitchell, *Chemphyschem*, 2007, **8**, 2036-2050.
3 Y. H. Xiang, D. M. Zhong, P. Wang, G. Y. Mao, H. H. Yu and S. X. Qu, *J. Mech. Phys. Solids*, 2018, **117,** 110-122.
4 H. Y. Ma and M. Zhang, *J. Mater. Sci.*, 2014, **49**, 8123-8126. 5 Y. Cai, Q. H. Lu, X. L. Guo, S. T. Wang, J. L. Qiao and L. Jiang, *Adv. Mater.*, 2015, **27**, 4162-4168.
6 W. T. Xu, C. F. Ma, J. L. Ma, T. S. Gan and G. Z. Zhang, *ACS Appl. Mater. Inter.*, 2014, **6**, 4017-4024.
7 X. Zheng, Z. Y. Guo, D. L. Tian, X. F. Zhang, W. X. Li and L. Jiang, *ACS Appl. Mater. Inter.*, 2015, **7**, 4336-4343.
8 M. J. Liu, S. T. Wang, Z. X. Wei, Y. L. Song and L. Jiang, *Adv. Mater.*, 2010, **21**, 665-669.
9 T. S. Wong, S. H. Kang, S. K. Y. Tang, E. J. Smythe, B. D. Hatton, A. G and J. Aizenberg, *Nature*, 2011, **477**, 443-447.

10 Y. Lu, S. Sathasivam, J. L. Song, C. R. Crick, C. J. Carmalt and I. P. Parkin, *Science*, 2015, **347**, 1132-1135.
11 K. Rykaczewski, A. T. Paxson, M. Staymates, M. L. Walker, X. D. Sun, S. Anand, S. Srinivasan, G. H. Mckinley, J. Chinn, J. H. J. Scott and K. K. Varanasi, *Sci. Rep.*, 2014, **4**, 4158.
12 M. Sun, R. B. Bai, X. Y. Yang, J. Q. Song, M. Qin, Z. G. Suo, X. M. He, *Adv. Mater.*, 2018, **30**, 1804916.
13 H. W. Chen, L. W. Zhang, P. F. Zhang, D. Y. Zhang, Z. W. Han and L. Jiang, *Small*, 2017, **13**, 1601676.
14 T. Du, S. H. Ma, X. W. Pei, S. T. Wang and F. Zhou, *Small*, 2016, **13**, 1602020.
15 J. B. Fan, Y. Y. Song, S. T. Wang, J. X. Meng, Y. Gao, X. L. Guo, L. Feng and L. Jiang, *Adv. Funct. Mater.*, 2015, **25**, 5368-5375.
16 Z. X. Xue, S. T. Wang, L. Lin, L. Chen, M. J. Liu, L. Feng and L. Jiang, *Adv. Mater.*, 2011, **23**, 4270-4273.
17 T. Matsubayashi, M. Tenjimbayashi, M. Komine, K. Manabe and S. Shiratori, *Ind. Eng. Chem. Res.,* 2017, **56**, 7080-7085.
18 D. M. Zhong, Y. H. Xiang, T. H. Yin, H. H. Yu and S. X. Qu, *Int. J. Solids Struct.*, 2019, **176-177**, 121-134.
19 B. B. Xu, Q. H. Liu, Z. G. Suo and R. C. Hayward, *Adv. Funct. Mater.*, 2016, **26**, 3218-3225.
20 D. Wang, N. Cheewaruangroj, Y. F. Li, G. McHale, Y. Z. Jiang, D. Wood, J. S. Biggins and B. B. Xu, *Adv. Funct. Mater.*, 2018, **28**, 1704228.
21 J. T. Muth, D. M. Vogt, R. L.Truby, Y. Mengüç, D. B. Kolesky, R. J. Wood and J. A. Lewis, *Adv. Mater.*, 2014 , **26**, 6307-6312.
22 H. Yang, C. H. Li, M. Yang, Y. D. Pan, Q. F. Yin, J. D. Tang, J. H. Qi and Z. G. Suo, *Adv. Funct. Mater.*, 2019, **29**, 1901721
23 M. Lei, W. Hong, Z. Zhao, C. M. Hamel, M. Chen, H.B. Lu and H. J. Qi, *ACS Appl. Mater. Inter.*, 2019, **11**, 22768-22776.
24 H. B. Lu, Y. Z. Liu, B. B. Xu, D. Hui and Y. Q. Fu, *Composites Part B: Engineering*, 2017, **122**, 9–15.
25 J. H. Guan, E. Ruiz-Gutierrez, B. B. Xu, D. Wood, G. McHale, R. Ledesma-Aguilar and G. G. Wells, *Soft Matter*, 2017, **13**, 3404-3410.
26 L. Z. Dood, D. Wood, N. R. Geraldi, G. G. Wells, G. McHale, B. B. Xu, S. Stuart-Cole, J. Martin and M. I. Newton, *ACS Appl. Mater. Inter.*, 2016, **8**, 22658-22663.
27 S. S. Yuan, J. Y. Zhu, Y. Li, Y. Zhao, J. Li, P. Van Puyvelde and B. Van der Bruggen, *J. Mater. Chem. A*, 2019, **7**, 2723-2729.
28 S. Y. Zhang, F. Lu, L. Tao, N. Liu, C. R. Gao, L. Feng and Y. Wei, *ACS Appl. Mater. Inter.*, 2013, **5**, 11971-11976.
29 Y. Dong, J. Li, L. Shi, X. B. Wang, Z. G. Guo and W. M. Liu, *Chem. Commun.*, 2014, **50**, 5586-5589.
30 Z. G. Xu, Y. Zhao, H. X. Wang, H. Zhou, C. X. Qin, X. G. Wang and T. Lin, *ACS Appl. Mater. Inter.*, 2016, **8**, 5661-5667.
31 Y. H. Xiang, D. M. Zhong, P. Wang, T. H. Yin, H. F. Zhou, H. H. Yu, C. Baliga, S. X. Qu and W. Yang, *J. Mech. Phys. Solids*, 2019, **208**, 208-218.

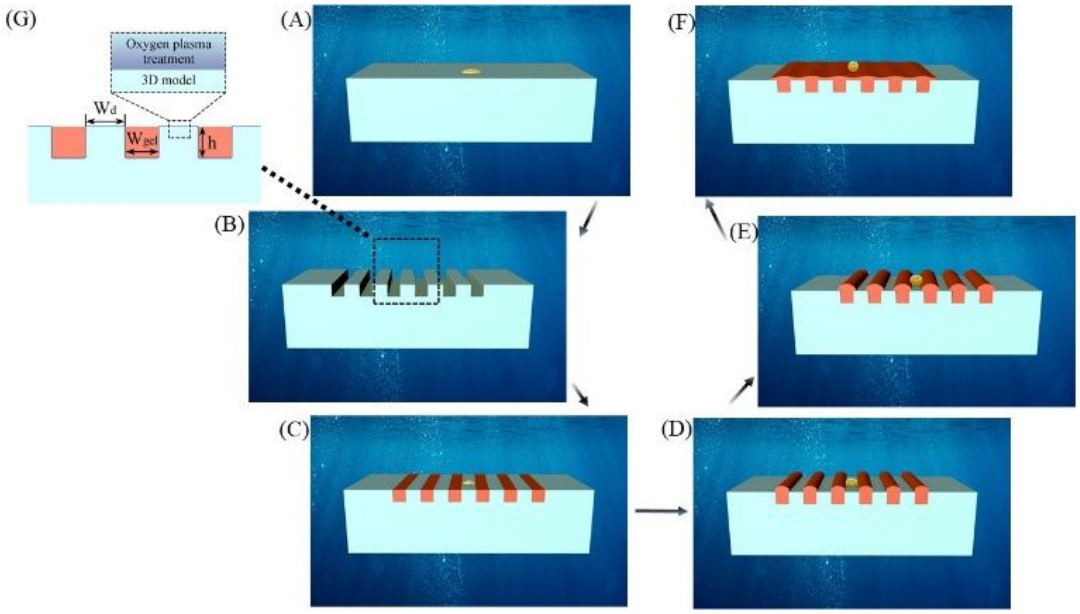

Fig. 1

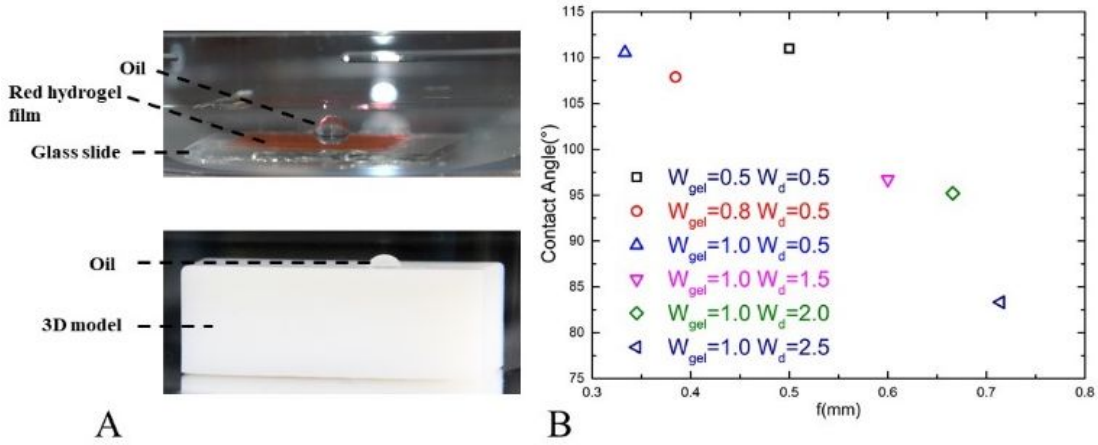
Oil
Red hydrogel film
Glass slide
Oil
3D model
A
B
Contact Angle(°)
f(mm)
W_gel=0.5 W_d=0.5
W_gel=0.8 W_d=0.5
W_gel=1.0 W_d=0.5
W_gel=1.0 W_d=1.5
W_gel=1.0 W_d=2.0
W_gel=1.0 W_d=2.5

Fig. 2

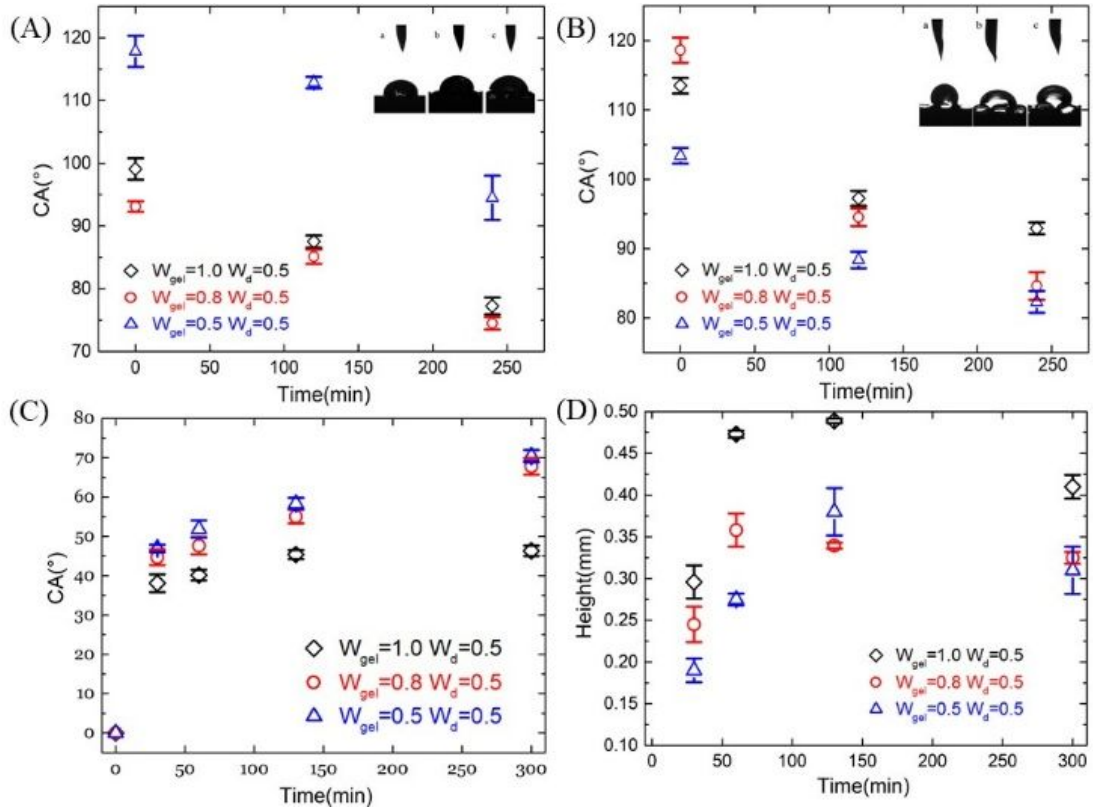
(A)
CA(°)
Time(min)
W_{gel}=1.0 W_d=0.5
W_{gel}=0.8 W_d=0.5
W_{gel}=0.5 W_d=0.5
(B)
CA(°)
Time(min)
W_{gel}=1.0 W_d=0.5
W_{gel}=0.8 W_d=0.5
W_{gel}=0.5 W_d=0.5
(C)
CA(°)
Time(min)
W_{gel}=1.0 W_d=0.5
W_{gel}=0.8 W_d=0.5
W_{gel}=0.5 W_d=0.5
(D)
Height(mm)
Time(min)
W_{gel}=1.0 W_d=0.5
W_{gel}=0.8 W_d=0.5
W_{gel}=0.5 W_d=0.5

Fig. 3

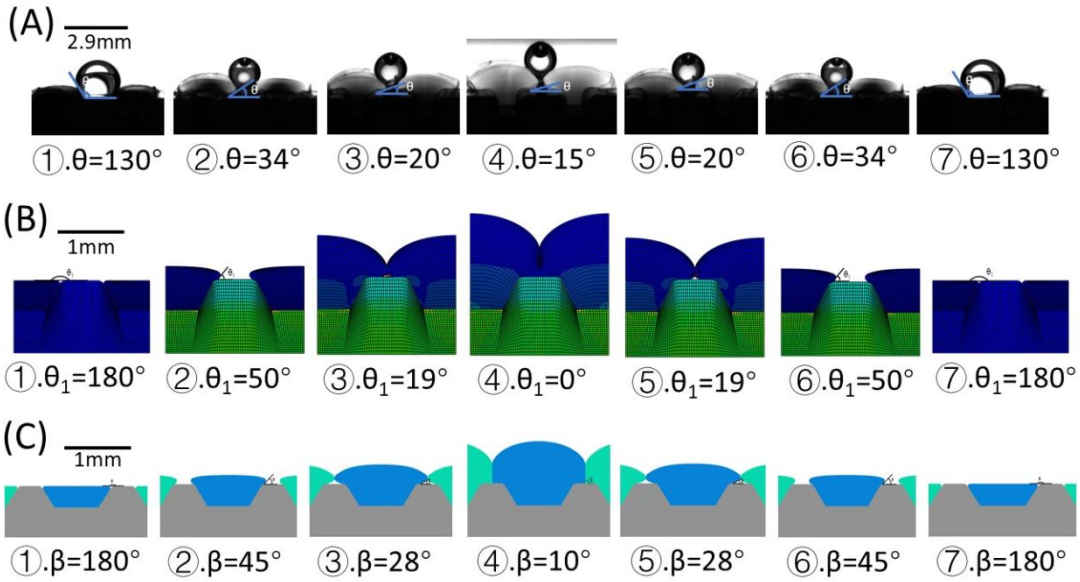
(A)
2.9mm
①.θ=130°
②.θ=34°
③.θ=20°
④.θ=15°
⑤.θ=20°
⑥.θ=34°
⑦.θ=130°
(B)
1mm
①.θ1=180°
②.θ1=50°
③.θ1=19°
④.θ1=0°
⑤.θ1=19°
⑥.θ1=50°
⑦.θ1=180°
(C)
1mm
①.β=180°
②.β=45°
③.β=28°
④.β=10°
⑤.β=28°
⑥.β=45°
⑦.β=180°

Fig. 4

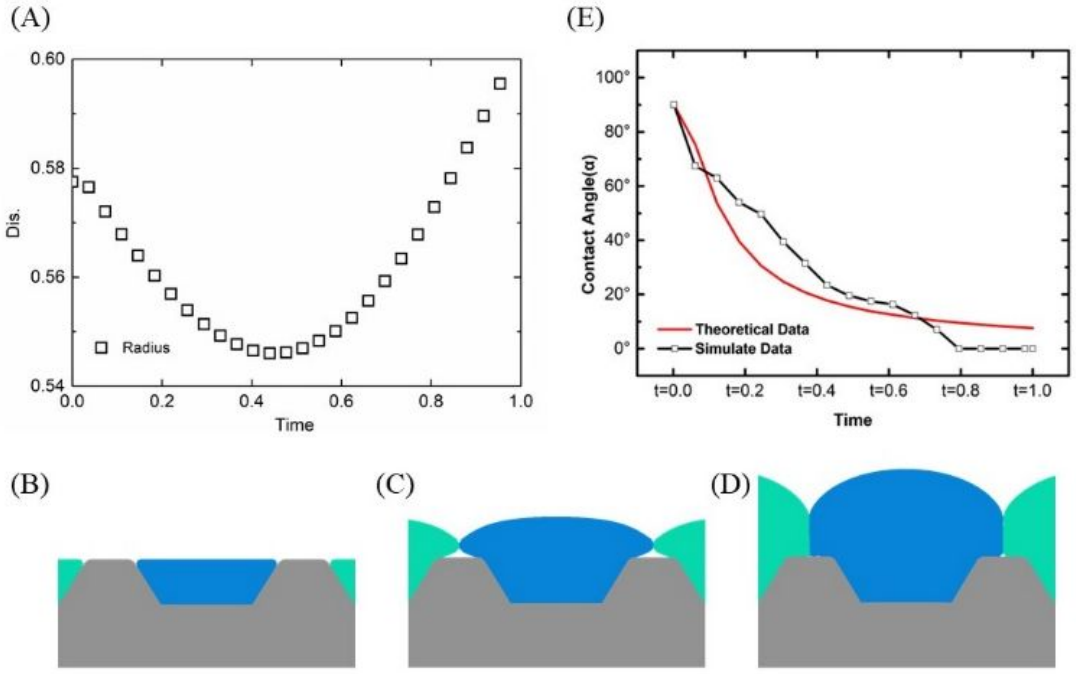
(A)
0.60
0.58
0.56
0.54
Dis.
Radius
0.0
0.2
0.4
0.6
0.8
1.0
Time
(E)
100°
80°
60°
40°
20°
0°
Contact Angle(α)
Theoretical Data
Simulate Data
t=0.0
t=0.2
t=0.4
t=0.6
t=0.8
t=1.0
Time
(B)
(C)
(D)

Fig. 5

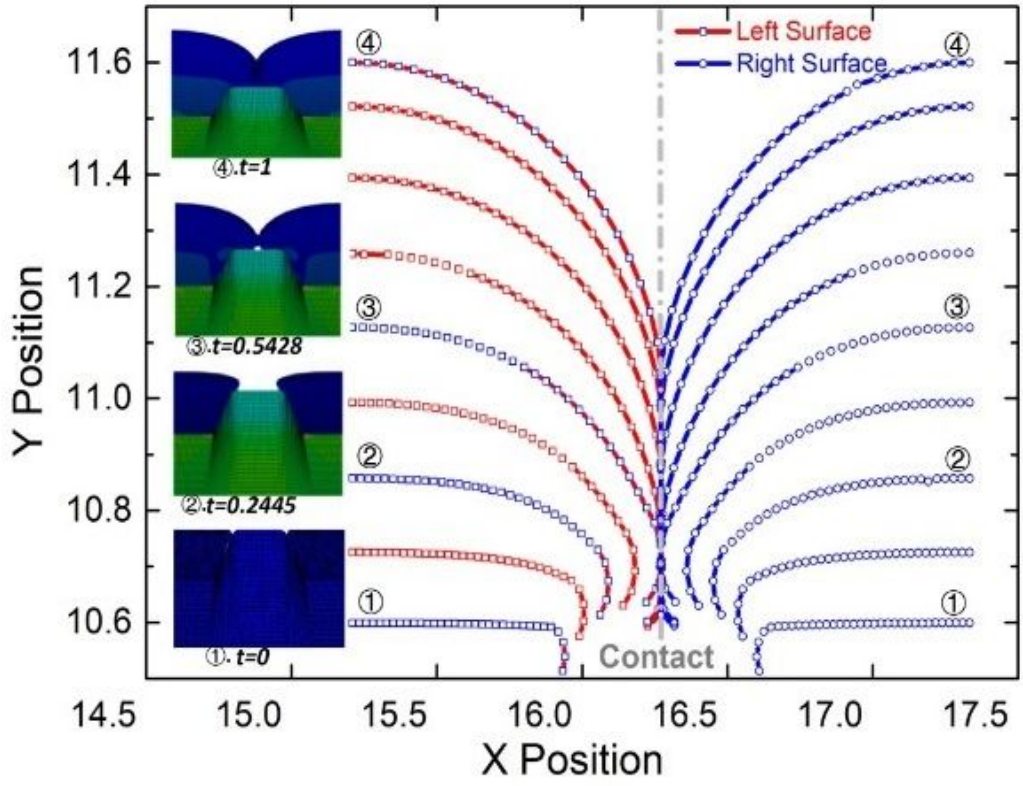
Left Surface
Right Surface
④
③
②
①
④.t=1
③.t=0.5428
②.t=0.2445
①. t=0
Contact
Y Position
X Position
11.6
11.4
11.2
11.0
10.8
10.6
14.5
15.0
15.5
16.0
16.5
17.0
17.5

Fig. 6

Stimuli-responsive gel impregnated surface with switchable lipophilic/oleophobic properties

Zhenghong Li[a], Yingzhi Liu[a], Ming Lei[a], Ansu Sun[b], Sreepathy Sridhar[b], Yifan Li[b], Xuqing Liu[c], Haibao Lu*[a], Yong Qing Fu[b] and Ben Bin Xu*[b]

a. State Key Laboratory of Science and Technology on Advanced Composites in Special Environments, Harbin Institute of Technology, Harbin 150080, P.R. China.

b. Smart Materials and Surfaces Laboratory, Faculty of Engineering and Environment, Northumbria University, Newcastle upon Tyne NE1 8ST, UK.

c. School of Materials, University of Manchester, Oxford Road, Manchester, United Kingdom, M13 9PL.

† E-mail: luhb@hit.edu.cn and ben.xu@northumbria.ac.uk

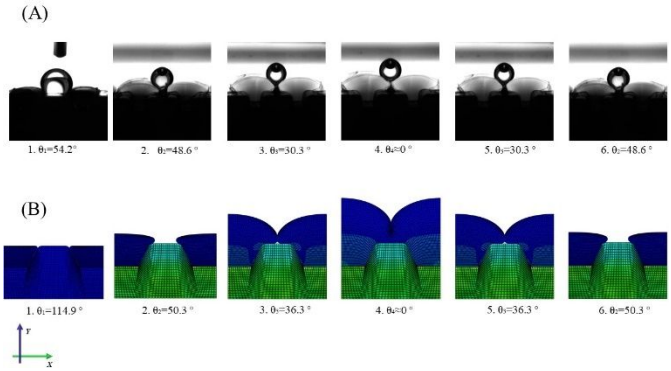

Stimuli-responsive gel impregnated surface with switchable lipophilic/oleophobic properties driven by swelling effect of hydrogel with controllable morphology.